RSC Advances

PAPER

View Article Online
View Journal | View Issue

Cite this: *RSC Adv.*, 2019, **9**, 32735

$ZnCl_2$ loaded TiO_2 nanomaterial: an efficient green catalyst to one-pot solvent-free synthesis of propargylamines†

Digambar B. Bankar,[ab] Ranjit R. Hawaldar,[a] Sudhir S. Arbuj,[a] Mansur H. Moulavi,[a] Santosh T. Shinde,[d] Shrikant P. Takle,[a] Manish D. Shinde,[a] Dinesh P. Amalnerkar[c] and Kaluram G. Kanade *[ac]

One-pot green synthesis of propargylamines using $ZnCl_2$ loaded TiO_2 nanomaterial under solvent-free conditions has been effectively accomplished. The aromatic aldehydes, amines, and phenylacetylene were reacted at 100 °C in the presence of the resultant catalyst to form propargylamines. The nanocrystalline TiO_2 was initially synthesized by a sol–gel method from titanium(IV) isopropoxide (TTIP) and further subjected to $ZnCl_2$ loading by a wet impregnation method. X-ray diffraction (XRD) patterns revealed the formation of crystalline anatase phase TiO_2. Field emission scanning electron microscopy (FESEM) showed the formation of agglomerated spheroid shaped particles having a size in the range of 25–45 nm. Transmission electron microscopy (TEM) validates cubical faceted and nanospheroid-like morphological features with clear faceted edges for the pure TiO_2 sample. Surface loading of $ZnCl_2$ on spheroid TiO_2 nanoparticles is evident in the case of the $ZnCl_2$ loaded TiO_2 sample. X-ray photoelectron spectroscopy (XPS) confirmed the presence of Ti^{4+} and Zn^{2+} species in the $ZnCl_2$ loaded TiO_2 catalyst. Energy-dispersive X-ray (EDS) spectroscopy also confirmed the existence of Ti, O, Zn and Cl elements in the nanostructured catalyst. 15% $ZnCl_2$ loaded TiO_2 afforded the highest 97% yield for 3-(1-morpholino-3-phenylprop-2-ynyl)phenol, 2-(1-morpholino-3-phenylprop-2-ynyl)phenol and 4-(1,3-diphenylprop-2-ynyl)morpholine under solvent-free and aerobic conditions. The proposed nanostructure-based heterogeneous catalytic reaction protocol is sustainable, environment-friendly and offers economic viability in terms of recyclability of the catalyst.

Received 25th August 2019
Accepted 7th October 2019

DOI: 10.1039/c9ra06693d

rsc.li/rsc-advances

1. Introduction

Organic reactions involving three or more components are becoming increasingly important day by day since they allow many starting materials to be combined easily in one-pot forming a single compound.[1] One-pot, multi-component carbon–carbon and carbon–nitrogen bond forming reactions were successfully accomplished for producing molecular complexity.[2] Three-component coupling of aldehyde, amine, and alkyne is one of the most extensively used methods for the preparation of several propargylamines through C–H bond activation.[3] Propargylamine derivatives play a significant role in synthetic organic chemistry by acting as a versatile intermediate for the synthesis of many biologically active heterocyclic compounds such as 2-aminoimidazoles,[4] pyrrolidines,[5] pyrroles,[6] phenanthrolines,[7] oxazolidinones,[8] aminoindolizines,[9] *etc.* Moreover, they are the important structural ingredients of therapeutic drug molecules and also of natural products.[10] For example, rasagiline containing Azilect as a moiety of propargylamine has been used for the symptomatic therapy in early Parkinson's disease.[11–13] Also, propargylamines are essential intermediates for the preparation of PF960IN as a biologically active drug molecule.[14]

The literature survey reveals that the synthesis of propargylamines *via* classical routes involves the addition of alkynyl-metal reagents to the imines[15,16] in the separate step. However, the addition of moisture sensitive Grignard or Li acetylides reagent is tedious. Through direct amination of propargylic electrophiles like propargyl halides, triflates and phosphates,[17] the formation of propargylamine derivatives also has been achieved.

In the last few decades, enormous progress has been made for the C–H bond activation of terminal alkynes. A variety of

[a]*Centre for Materials for Electronics Technology (C-MET), Panchwati, Off Pashan Road, Pune-411008, India. E-mail: kgkanade@yahoo.co.in*

[b]*P. G. Department of Chemistry, R. B. Narayanrao Borawake College, Shrirampur, Ahmednagar-413709, India*

[c]*P. G. and Research Centre, Yashavantrao Chavan Institute of Science, Satara-415001, India*

[d]*P. G. Department of Chemistry, Annasaheb Awate College, Manchar, Pune-410503, India*

† Electronic supplementary information (ESI) available. See DOI: 10.1039/c9ra06693d

homogeneous transition metallic systems such as Cu(I) salts,[18] Ag(I) salts,[19] $ZnMe_2$,[20] Fe(III) salts,[21] Cu(I) salts,[22] Zr complex,[23] Ni(II) salts,[24] $InCl_3$,[25] Ir complex[26] and AgOAc[27] were used for the C–H bond activation of terminal alkynes. Researchers also used Cu–Ru bimetallic system,[28] $InBr_3$,[29] Co(II)[30] and Au(III) salen complexes[31] as a homogeneous catalytic system for the activation of C–H bond of the terminal alkynes. However, some of these catalytic systems have certain limitations due to the use of expensive and excess amount of catalyst, toxic solvents, and the requirement of inert atmospheric conditions.

Diverse heterogeneous catalysts such as layered double hydroxide-supported gold (LDH-$AuCl_4$) catalyst,[32] polystyrene-supported NHC–Ag(I) catalyst,[33] Fe_3O_4 nanoparticles,[34] Ag nanoparticles/Ni metal–organic framework,[35] copper(I) anchored onto MCM-41 silica,[36] Fe_3O_4@SBA-15 (ref. 37) *etc.* were used for the synthesis of propargylamines. Nanoscale metal oxides such as ZnO[38] and In_2O_3 (ref. 39) were also used for the synthesis of propargylamines. Further, copper ferrite nanoparticles,[40] Ni–Y zeolites,[41] nanosize Co_3O_4,[42] Cu nanoparticles on TiO_2,[43] Au nanoparticles supported on ionic liquid,[44] Au nanoparticles supported on polyacrylamide,[45] Zn(II)/HAP/Fe_3O_4,[46] Zn(L-proline)$_2$,[47] *etc.* were used as heterogeneous catalysts for the three component synthesis of propargylamines. Besides, a super paramagnetic MCM-41 with dendrites copper complex[48] was utilized as a recyclable catalyst for the propargylamine synthesis. Nonetheless, there are disadvantages to some of such catalytic systems *viz.* requirement of high catalyst amount, use of inert gas, use of solvent, longer reaction time, *etc.* Hence, there is a need to find a simple and efficient method for the synthesis of propargylamines.

In the context of heterogeneous catalysis, nanocrystalline materials can play significant role due to their large surface to volume ratio, easy separation and desirable physico-chemical characteristics.[49] Specifically, nanocrystalline TiO_2 is one of the most important materials extending widespread applications in pigments, catalytic systems, inorganic membranes, gas sensors, support ceramics,[50] *etc.* Also, non-toxic nature and low cost of TiO_2 nano-particulate system made it a better catalyst. The TiO_2 supported with transition metals brings the advantage of heterogeneous catalysis in the propargylamine synthesis. Fe doped TiO_2 nanoparticles are used as a heterogeneous catalyst for the activation of C–H bond of terminal alkynes under microwave irradiation.[51] Recently, Ag/TiO_2 and Pt/TiO_2 nanocatalyst have been applied as active recyclable catalysts for the synthesis of propargylamines under microwave irradiation at 140 °C.[52]

Effective use of zinc salts[53] for the propargylamine synthesis motivated us to perform one-pot synthesis of propargylamine using $ZnCl_2$ loaded TiO_2 nanomaterial.

In this report, we have demonstrated a synthetic strategy in which inexpensive and commercially available $ZnCl_2$ is loaded by wet impregnation technique on sol–gel generated TiO_2 nanoparticles. The as-synthesized nanocrystalline $ZnCl_2$ loaded TiO_2 has been used as an efficient and green heterogeneous catalyst for the synthesis of propargylamines under solvent-free and aerobic conditions.

2. Experimental

2.1. General

All the chemicals were AR grade and purchased from a local dealer. The chemicals were used as received without further purification. The progress of reaction was monitored by thin layer chromatography (TLC) technique. The crystal structure of the synthesized catalyst was detected by XRD using a Rigaku MiniFlex-600 diffractometer (Cu Kα radiation, $\lambda = 1.5406$ Å). The surface morphology and particle size were examined using field emission scanning electron microscope (Hitachi S-4800). Elemental compositions were determined by energy-dispersive X-ray spectroscopy (EDS) analysis. For fine-scale nanostructural evaluation, field emission transmission electron microscopic (FETEM) images of the typical sample were obtained using the JEOL JEM-2200 FS instrument. The same instrument was also used for obtaining the Energy Dispersive Spectroscopy (EDS) and allied elemental mapping information using scanning transmission electron microscopy (STEM) in bright field mode. For the confirmation of chemical composition, X-ray photoelectron spectroscopic (XPS) scans were recorded using Al Kα (Monochromatic) anode with 6 mA beam current and 12 kV X-ray source. The as-synthesized propargylamine derivatives were spectrally characterized by Nuclear Magnetic Resonance (NMR) spectroscopy and High-Resolution Mass Spectrometry (HRMS) techniques. ^{1}H and ^{13}C NMR spectra were recorded using $CDCl_3$ and DMSO-d_6 solvents on 500 and 125 MHz Bruker NMR spectrometer, respectively. The HRMS was taken in methanol solvent using high-resolution mass spectrometer (Bruker Germany, Model: Impact HD, UHR Impact II ESI-Q-TOF). All yields refer to the isolated products after purification by column chromatography with ethyl acetate and *n*-hexane as an eluent.

2.2. Synthesis of TiO_2 nanoparticles

Synthesis of TiO_2 nanoparticles was performed by sol–gel method using titanium(IV) isopropoxide as a titanium precursor. Initially, 80 ml of glacial acetic acid was added dropwise to a 40 ml of titanium(IV) isopropoxide (TTIP) in a 500 ml round bottom flask immersed in an ice bath with constant stirring. Later, 100 ml isopropyl alcohol was gradually added with vigorous stirring for a period of 30 min at room temperature. In the resulting solution, 10 g polyvinyl alcohol (PVA) in 50 ml isopropyl alcohol was added, stirred for 10 min and subsequently, 10 ml of 1 M HCl was added and the resultant solution was subjected to constant stirring at room temperature for 4 h. For natural gel formation, the obtained mixture was transferred into 500 ml beaker and kept for 5 days. Finally, the gel was dried at 110 °C for 12 h, transferred into a mortar, powdered with pestle and further calcined in a muffle furnace at 400 °C for 4 h.

2.3. Synthesis of $ZnCl_2$ loaded TiO_2 nanomaterial ($ZnCl_2$–TiO_2 catalyst)

Loading of 15 wt% $ZnCl_2$ over TiO_2 nanoparticles was performed by wet impregnation technique. A mixture of $ZnCl_2$ (0.3

g) and TiO_2 nanoparticles (2.0 g) was grinded for 10 min and subsequently transferred into the 250 ml round bottom flask containing 50 ml ethanol. Further, it was stirred at room temperature for 1 h and then refluxed for 4 h with persistent stirring. The excess ethanol was concentrated under vacuum distillation and obtained solid material was dried at 200 °C for 6 h. The same procedure was repeated for the loading of 5 wt%, 10 wt% and 20 wt% $ZnCl_2$ over TiO_2 nanoparticles.

2.4. General procedure for the synthesis of propargylamine derivatives

In a typical procedure, aromatic aldehyde (1 mmol), secondary amine (1.2 mmol) and phenylacetylene (1.5 mmol) were taken in a clean and oven-dried round bottom flask. The nanocrystalline $ZnCl_2$–TiO_2 catalyst (0.2 mmol) was added into the round bottom flask and the resulting reaction mixture was placed in pre-heated oil bath at 100 °C and stirred at the same temperature for 6 h. Progress of the reaction was checked by thin layer chromatography (TLC). After cooling, ethyl acetate was added to the reaction mass and stirred at room temperature for 15 min. Ethyl acetate layer was separated by filtration and again remaining reaction residue was washed with ethyl acetate. Combined ethyl acetate washings were mixed with water. The organic layer was separated by extraction, dried over anhydrous Na_2SO_4 and filtered. The organic solvent was concentrated under reduced pressure and obtained crude residue was purified by column chromatography to yield the desired propargylamine derivative. The pure organic compounds were characterized by ^{1}H NMR, ^{13}C NMR, and HRMS spectral techniques (please see ESI†).

3. Results and discussion

3.1. Catalyst characterization

3.1.1. XRD analysis. Fig. 1 depicts the XRD patterns of pure TiO_2 and $ZnCl_2$–TiO_2 nanostructures. The characteristic peaks with 2θ values at 25.26°, 37.70°, 48.07°, 53.86°, 55.00°, 62.68°, 68.76°, 70.26° and 75.06° can be indexed as (101), (004), (200), (105), (211), (204), (116), (220) and (215) planes corresponding to anatase polymorph of TiO_2 (Fig. 1a). The angular positions and relative intensities of all the diffraction peaks are in close concurrence with the JCPDS card no. 21-1272 for anatase phase of TiO_2. The XRD peak patterns corresponding to 5%, 10%, 15% and 20% $ZnCl_2$ loaded TiO_2 samples also exhibit formation of anatase phase of TiO_2 (Fig. 1b–e). Furthermore, no additional peaks other than those matching with the crystalline anatase TiO_2 were found in the XRD, indicating the phase purity of the synthesized materials. It has been observed that 2θ values are slightly shifted to higher values for $ZnCl_2$ loaded TiO_2 samples in comparison to pure TiO_2 implying successful loading of $ZnCl_2$ over TiO_2 surface as shown in inset of Fig. 1 for (101) plane. The 2θ values of (101) plane for pure TiO_2, 5% and 10% $ZnCl_2$–TiO_2 samples are almost the same (around 25.26°, 25.28° and 25.26°, respectively). For higher loading *i.e.* 15% and 20% $ZnCl_2$–TiO_2, the 2θ values of (101) plane are observed to be around 25.42° and 25.44°, respectively. The XRD peaks due to zinc species could not be observed, as expected, due to low concentration and highly uniform dispersion of Zn species over the nanocrystalline TiO_2.[54]

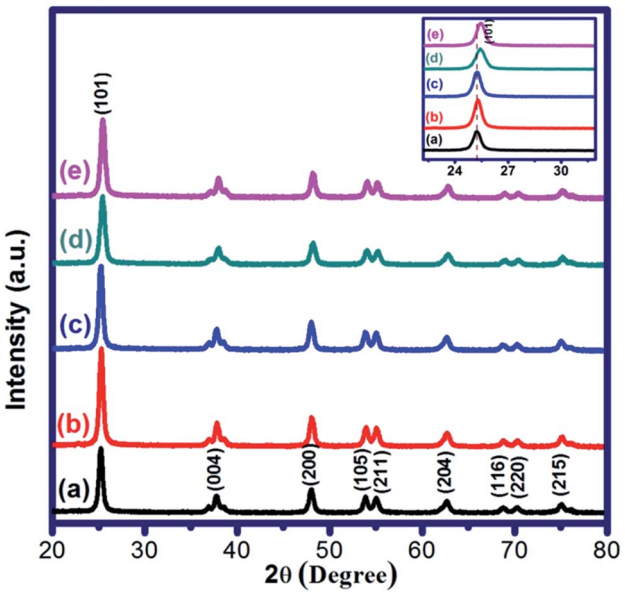

Fig. 1 XRD patterns of (a) pure TiO_2, (b) 5% $ZnCl_2$–TiO_2, (c) 10% $ZnCl_2$–TiO_2, (d) 15% $ZnCl_2$–TiO_2 and (e) 20% $ZnCl_2$–TiO_2. Inset is enlarged view of (101) plane.

The crystallite size of all as-synthesized samples was calculated by Scherrer's equation using broadening of (101) anatase peak of TiO_2. The crystallite size of unloaded TiO_2 is 16 nm, whereas 5%, 10%, 15% and 20% $ZnCl_2$ loaded TiO_2 showed crystallite size values of 16, 15, 13 and 14 nm respectively. It may be, however, noted that there is no prominent change in the overall crystallite size of all the samples under investigation. The miniscule decrease in crystallite size of $ZnCl_2$–TiO_2 in comparison to pure TiO_2 as well as the marginal shift in 2θ value of (101) plane with increasing loading percentage of $ZnCl_2$ on TiO_2 nanoparticles can be ascribed to the effective surface coating of $ZnCl_2$ over TiO_2 and/or might be due to partial incorporation of Zn species in the crystalline lattice of TiO_2.

3.1.2. FESEM analysis. The surface morphology of the pure TiO_2 and 15% $ZnCl_2$–TiO_2 was investigated by FESEM analysis and images are shown in the Fig. 2. Pure TiO_2 sample displays the formation of homogeneously distributed spheroidal shaped particles having size in the range of 15–30 nm (Fig. 2a and b). In case of 15% $ZnCl_2$–TiO_2 sample (Fig. 2c and d), almost same morphology is observed with increased particle size (25–45 nm) as compared to pure TiO_2 due to agglomeration of particles and surface coating/loading of TiO_2 nanoparticles by $ZnCl_2$.

3.1.3. FETEM analysis. Fig. 3 displays FETEM images corresponding to pure TiO_2 and 15% $ZnCl_2$ loaded TiO_2 nanomaterials. Low and intermediate magnification FETEM images (Fig. 3a and b) show cubical faceted and spheroid-like morphological features with clear faceted edges for pure TiO_2 sample. Occasionally, nanorods like features are also seen. Surface coating/loading of spheroid particles of TiO_2 by $ZnCl_2$ is visible in case of $ZnCl_2$ loaded TiO_2 sample when compared

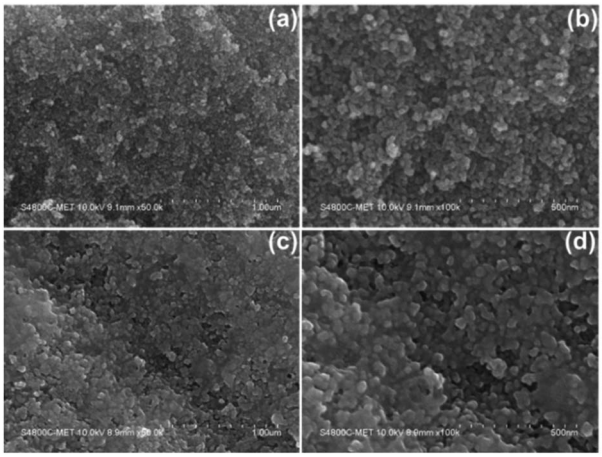

Fig. 2 FESEM images of (a and b) Pure TiO_2 and (c and d) 15% $ZnCl_2$–TiO_2.

with pure TiO_2 sample. The average particle size for TiO_2 and $ZnCl_2$–TiO_2 was found to be in the range of 15–35 nm. The lattice fringes with inter-planar spacing (d) of 0.365 nm (Fig. 3c) and 0.369 nm (Fig. 3g), respectively, for pure and $ZnCl_2$–TiO_2 samples corresponding to (101) plane of anatase TiO_2 are seen.[55] The lattice fringes corresponding to (105), (103), (004), (200), *etc.* planes are also noticed in case of both the samples which is an indication of polycrystalline nature of the samples. The selected area electron diffraction (SAED) patterns as shown in Fig. 3(d and h) evince nanocrystalline behaviour of the samples showing presence of ring like patterns, however, such rings are not continuous but are dominated by the regular bright spots.[56] SAED patterns confirm anatase phase TiO_2 in case of both the samples when compared with XRD diffractograms and allied database (Fig. 1). The overall FETEM study revealed formation of nanoscale spheroids exhibiting nanocrystalline nature.

3.1.4. FETEM-STEM-EDS analysis of $ZnCl_2$–TiO_2 catalyst. The energy dispersive X-ray spectroscopy (EDS) analysis was used for the confirmation and quantification of presence of elements in the given sample in STEM mode. In our investigation, weight by weight amount of $ZnCl_2$ and TiO_2 were used in the wet impregnation method. For TEM-EDS elemental composition analysis, we considered 15% $ZnCl_2$–TiO_2 sample and the relevant spectrum with quantitative data (in tabular form) is reproduced in Fig. 4.

The EDS spectrum discloses that the 15% $ZnCl_2$–TiO_2 catalyst contains 33.36 wt% of oxygen, 6.08 wt% of chlorine, 43.29 wt% of titanium and 17.27 wt% of Zn, even though the XRD pattern did not show any Zn peaks. Thus, EDS spectrum revealed that the sample is composed of Ti, O, Zn, and Cl which is in good agreement with results obtained by XPS (Fig. 6).

The EDS-elemental mapping images of 15% $ZnCl_2$–TiO_2 sample in scanning transmission electron microscopy (STEM) mode are shown in Fig. 5.

The elemental mapping images due to Ti and O (Fig. 5b and c, respectively) overlap well with corresponding electron image (Fig. 5a). The intensity of the colours assigned to Ti and O is also very high. The elemental mapping images for Zn and Cl (Fig. 5d and e, respectively) also overlap with the corresponding electron image, however, the intensity of the colours ascribable to these

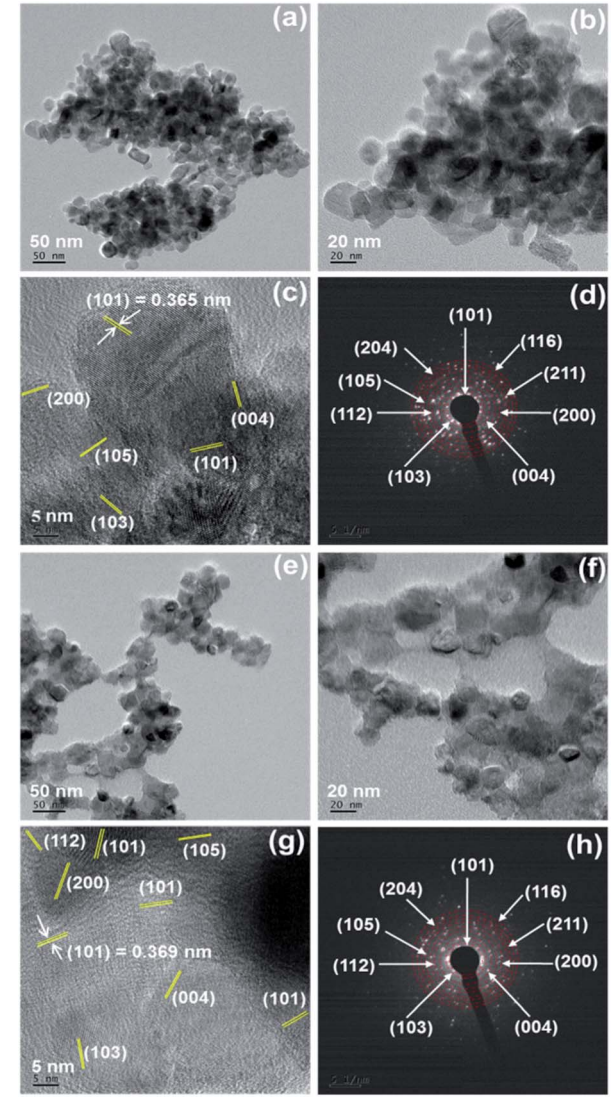

Fig. 3 TEM images: (a and b) pure TiO_2, (e and f) 15% $ZnCl_2$–TiO_2. HRTEM images: (c) TiO_2, (g) 15% $ZnCl_2$–TiO_2. (d and h) are the corresponding SAED patterns of TiO_2 and 15% $ZnCl_2$–TiO_2.

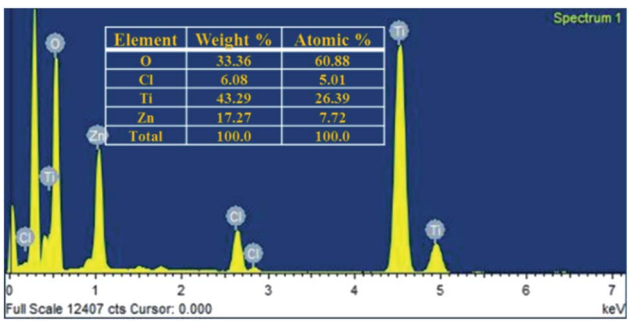

Fig. 4 TEM-EDS spectrum exhibiting quantitative elemental composition data for nanostructured 15% $ZnCl_2$–TiO_2.

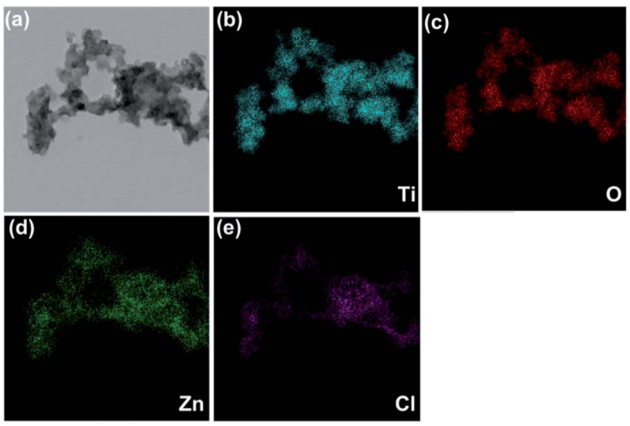

Fig. 5 FETEM-STEM-EDS elemental mapping images of 15% $ZnCl_2$–TiO_2 catalyst: (a) Electron image (b) Ti, (c) O, (d) Zn and (e) Cl.

two elements is low which is quite obvious as $ZnCl_2$ is used only for the purpose of surface loading. FETEM images correspond well with FESEM images and endorse the surface loading of $ZnCl_2$ over TiO_2 nanoparticles.

3.1.5. XPS analysis. XPS scans of the nanostructured $ZnCl_2$–TiO_2 were acquired to determine the elemental composition and the electronic state of the Ti, O, Zn and Cl elements. Fig. 6 shows the high resolution XPS scans corresponding to 15% $ZnCl_2$–TiO_2 sample. The binding energies were corrected with respect to the peak for adventitious C 1s at 284.8 eV. High resolution scans of core level Ti 2p, Zn 2p and Cl 2p exhibit symmetrical single peaks, while core level O 1s exhibits asymmetry due to ensemble of two peaks as noticed in its deconvolution spectrum.

The Ti binding energy peaks observed at 458.72 and 464.35 eV are related to Ti $2p_{3/2}$ and Ti $2p_{1/2}$, in close resemblance with that of Ti^{4+} in TiO_2.[57] The two O 1s peaks (inset of Fig. 6b) can be assigned to lattice oxygen (O–Ti) at 529.80 eV and surface-bound hydroxyl group (Ti–OH) at 531.78 eV. The binding energy peaks at 1022.20 eV and 1045.20 eV can be associated with Zn $2p_{3/2}$ and Zn $2p_{1/2}$ energy states, respectively (Fig. 6c). The peak at 1022.20 eV could be assigned to Zn^{2+} species in ZnO (1021.9 eV),[58] $ZnCl_2$ (1022.5 eV)[59] or $Zn(OH)_2$ (1022.6).[60] Subsequently, we studied the chloride XPS peak (Fig. 6d) to detect the presence of Zn^{2+} species among the ZnO, $ZnCl_2$ or $Zn(OH)_2$. The binding energy at 199.59 eV signifies the Cl $2p_{3/2}$ energy state of metal chloride. It apparently confirms the presence of $ZnCl_2$ (ref. 61) confined to surface in the $ZnCl_2$–TiO_2 catalyst (since XPS is surface sensitive technique).

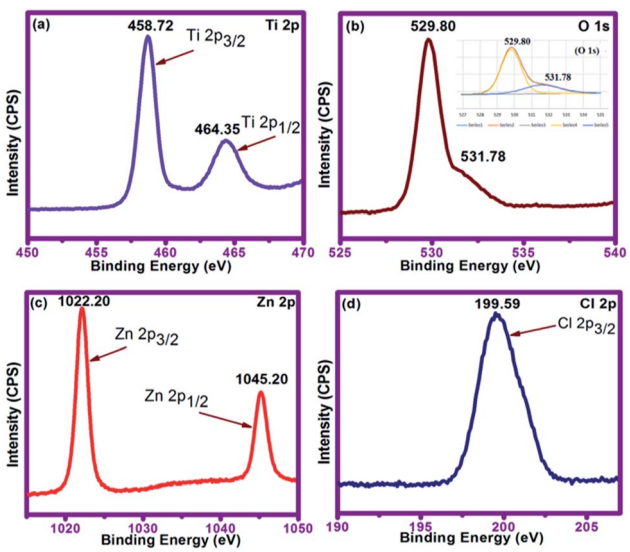

Fig. 6 High resolution XPS scans of the respective elements corresponding to 15% $ZnCl_2$–TiO_2 sample. The inset of (b) displays deconvoluted spectrum.

The overall appearance of peaks in XPS scans demonstrates the successful loading of $ZnCl_2$ on the surface of TiO_2 nanoparticles.

3.2. Catalytic activity of $ZnCl_2$ loaded TiO_2 nanomaterial

After successful synthesis and characterization of $ZnCl_2$–TiO_2 catalysts, it is employed as heterogeneous catalyst in multicomponent synthesis of propargylamine. To optimize the reaction conditions, several parameters such as catalyst, temperature and time were studied and corresponding results are summarized in Table 1. To achieve sustainable green chemistry approach, prior reaction was set under solvent-free and aerobic conditions. In the initial optimizations, 3-hydroxybenzaldehyde, morpholine, and phenylacetylene were used as substrates for the model reaction (Scheme 1).

When the reaction was performed at 30 °C in the presence of commercial $ZnCl_2$, no product formation was observed even after 6 h (Table 1, entry 1). However, when the reaction was carried out at 70 °C, low yield of product was obtained in 6 h (Table 1, entry 2). In addition, an increase in yield (76%) was observed as the temperature was raised to 100 °C (Table 1, entry 3). This indicates that the temperature plays an important role in this reaction. The lower yield using commercial $ZnCl_2$ can be due to its hygroscopic

Table 1 Optimization of catalyst, temperature and time for model reaction between 3-hydroxybenzaldehyde, morpholine and phenylacetylene[a]

Entry	Catalyst	Temp. (°C)	Time (h)	Yield[b] (%)
1	$ZnCl_2$	30 °C	6.0	—
2	$ZnCl_2$	70 °C	6.0	53
3	$ZnCl_2$	100 °C	6.0	76
4	Pure TiO_2	100 °C	6.0	38
5	5% $ZnCl_2$–TiO_2	100 °C	6.0	76
6	10% $ZnCl_2$–TiO_2	100 °C	3.0	57
7	10% $ZnCl_2$–TiO_2	100 °C	6.0	86
8	15% $ZnCl_2$–TiO_2	30 °C	6.0	—
9	15% $ZnCl_2$–TiO_2	70 °C	6.0	74
10	15% $ZnCl_2$–TiO_2	100 °C	3.0	68
11	15% $ZnCl_2$–TiO_2	100 °C	6.0	97
12	20% $ZnCl_2$–TiO_2	100 °C	6.0	97

[a] Reaction conditions: 3-hydroxybenzaldehyde (1 mmol), morpholine (1.2 mmol), phenylacetylene (1.5 mmol), catalyst (0.2 mmol), temp., time, solvent-free condition. [b] Isolated yield.

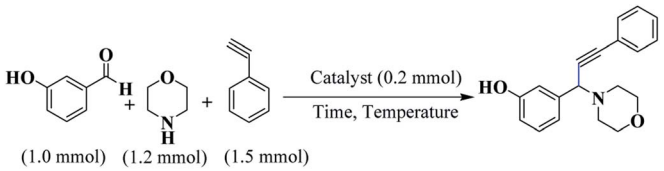

Scheme 1 Model reaction.

nature. We also performed the reaction using pure TiO_2, but observed only 38% yield (Table 1, entry 4).

Subsequently, the catalytic activities of 5%, 10%, 15% and 20% $ZnCl_2$ loaded TiO_2 nanoparticles (nanocrystalline $ZnCl_2$–TiO_2 catalysts) were examined. For 5% and 10% $ZnCl_2$ supported TiO_2 catalysts, yields of 76% and 86%, respectively, were obtained (Table 1, entries 5 and 7). This means that as the loading of $ZnCl_2$ on TiO_2 increases, an increase in product yield is observed under a constant mmol of catalyst (0.2 mmol). Therefore, we studied the reaction with 15% $ZnCl_2$ loaded TiO_2. No product formation was detected at 30 °C using 15% $ZnCl_2$ loaded TiO_2 catalyst (Table 1, entry 8), 74% yield obtained at 70 °C in 6 h (Table 1, entry 9), 68% yield obtained at 100 °C in 3 h (Table 1, entry 10). However, when the reaction was performed at 100 °C for 6 h, 97% yield of the desired product was observed (Table 1, entry 11). 15% $ZnCl_2$ loading over TiO_2 was necessary as the optimum amount of $ZnCl_2$ loading and increasing the loading of $ZnCl_2$ (20%) did not improve the yield (Table 1, entry 12).

It is clearly noticed that the nanostructured $ZnCl_2$–TiO_2 system exhibits excellent catalytic activity after loading $ZnCl_2$ over TiO_2 nanoparticles. The excellent catalytic activity of the nanostructured $ZnCl_2$–TiO_2 can be attributed to the greater degree of crystallinity at nanoscale.

It is very interesting to see the effect of solvents on catalytic activity of 15% $ZnCl_2$–TiO_2 catalyst. Therefore, we investigated the role of various solvents such as toluene, CH_3CN, DMF, THF, and H_2O.

From Table 2, is very clear that catalyst exhibits poor activity in polar solvents (CH_3CN, DMF, H_2O and THF). Non-polar solvent (toluene) shows good catalytic activity, while under solvent-free conditions, catalyst shows excellent catalytic activity. The reason for lowering the yield of propargylamine and hence catalytic activity lies in solvation of reactants and catalyst. In solvent, reactants are dispersed so it delays the contact with the catalyst. Under solvent-free conditions, reactants and catalyst can quickly come in intimate contact with each other which, in turn, can accelerate the reaction on the surface of the catalyst. Thus, best results could be observed for 15% $ZnCl_2$ loaded TiO_2 nanoparticle catalyst with 97% yield under solvent-free conditions.

Table 2 Solvent study for model reaction[a]

Entry	Solvent	Yield[b] (%)
1	Toluene	76
2	CH_3CN	68
3	DMF	40
4	H_2O	36
5	Solvent-free	97
6	THF	44

[a] Reaction conditions: 3-hydroxybenzaldehyde (1 mmol), morpholine (1.2 mmol), phenylacetylene (1.5 mmol), $ZnCl_2$–TiO_2 (0.2 mmol), 100 °C, 6.0 h, solvent. [b] Isolated yield.

After optimization of the reaction parameters, we have extended the scope of reaction to the different aromatic aldehydes, cyclic secondary amines (pyrrolidine and morpholine), and phenylacetylene using 15% $ZnCl_2$–TiO_2 (Scheme 2 and Table 3, entries 1–12).

The results in Table 3 indicate that the aromatic aldehydes with electron-donating and halogen substituents showed high reactivity and produced the corresponding propargylamines in better yields. Aryl aldehydes with a hydroxyl group at *meta* or *ortho* positions (Table 3, entries 1, 4 and 5), afforded excellent yields as compared to aldehydes having methoxy group at *para* position (Table 3, entries 2 and 3). The reactivity of 2-chloro and 4-chlorobenzaldehydes (Table 3, entries 9–11) was found to be slightly more than 4-flourobenzaldehyde (Table 3, entry 8) and 4-bromobenzaldehyde (Table 3, entry 12). Benzaldehyde afforded the coupling products in excellent yield (Table 3, entries 6 and 7). We observed slightly higher yields of the products using morpholine as compared to pyrrolidine. Thus, 15% $ZnCl_2$–TiO_2 catalyst worked as an efficient catalyst for the synthesis of propargylamines under solvent-free conditions. It may be noted that, the as-synthesized propargylamines are all chiral compounds and spectral data of all products confirmed that they are single compounds and not mixture of isomers.

The reusability of the $ZnCl_2$–TiO_2 catalyst was also examined for the reaction between 3-hydroxybenzaldehyde, morpholine, and phenylacetylene under the optimized reaction conditions (Table 3, entry 1). After the first run, the solid catalyst was separated from the reaction mixture by filtration, washed with the ethyl acetate and dried at 120 °C for 4 h. The dried catalyst was then subjected to the next run of the reaction under optimized conditions and afforded 94% yield. Similar procedure was followed for next runs. The relevant results are presented in Table 4. As can be seen, the catalyst could be recycled for five successive runs without significant loss of catalytic activity.

The recycled $ZnCl_2$–TiO_2 catalyst was further characterized by XRD which confirms retention of anatase phase of TiO_2 (Fig. S1, ESI†). It is, thus, noted that the crystal structure of the

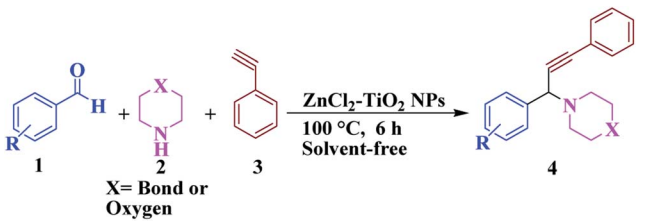

Scheme 2 General reaction for propargylamine synthesis.

Table 3 Propargylamine synthesis by three-component coupling of aromatic aldehyde, secondary amines and phenylacetylene catalysed by $ZnCl_2$–TiO_2 NPs[a]

Entry	Aldehyde	Product	Yield[b] (%)
1	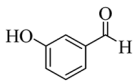	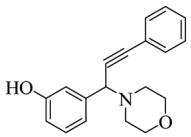	97
2	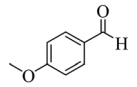	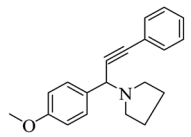	88
3	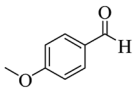	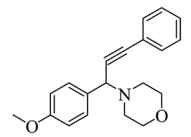	90
4	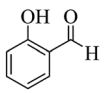	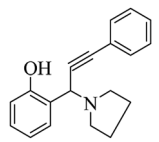	94
5	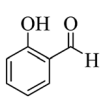	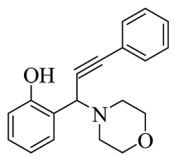	97
6	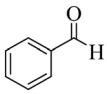	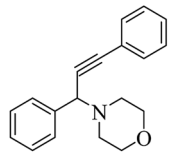	97
7	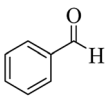	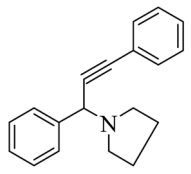	95
8	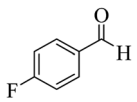	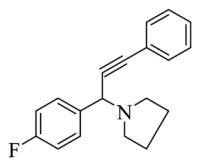	90
9	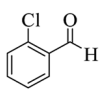	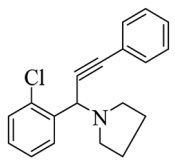	92
10	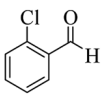	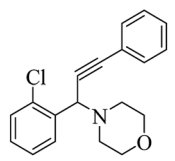	94

Table 3 (*Contd.*)

Entry	Aldehyde	Product	Yield[b] (%)
11	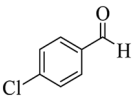	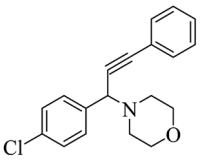	95
12	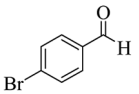	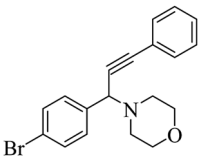	91

[a] Reaction conditions: aromatic aldehyde (1 mmol), amine (1.2 mmol), phenylacetylene (1.5 mmol), $ZnCl_2$–TiO_2 (0.2 mmol), 100 °C, 6.0 h, solvent-free condition. [b] Isolated yield.

recovered catalyst has not changed. The sharp peaks signify that the nature of recovered catalyst is crystalline.

The transition metals are generally used to activate the C–H bond of terminal alkynes in carbon–carbon coupling reactions. The transition metal supported on solid support such as TiO_2 nanoparticles might bring the advantage of heterogeneous catalysis in C–C bond forming reactions.[51] In the proposed reaction, the $ZnCl_2$ loaded TiO_2 nanomaterial ($ZnCl_2$–TiO_2) can also lead to activation of C–H bond of terminal alkyne. A tentative mechanism for the one-pot propargylamine synthesis under solvent-free condition using $ZnCl_2$ loaded TiO_2 nanomaterial is pictorially demonstrated in Scheme 3. The reaction initially involves activation of C–H bond of phenylacetylene (3) by $ZnCl_2$ from the nanostructured $ZnCl_2$–TiO_2 catalyst. The generated phenylacetylide–$ZnCl_2$–TiO_2 intermediate (a) is then reacted with iminium ion (b) (which is produced *in situ* from aldehyde 1 and amine 2) in order to offer the desired product of propargylamine 4. Here, $ZnCl_2$ in the $ZnCl_2$–TiO_2 nanomaterial is the main species to activate the C–H bond of terminal alkynes and anatase TiO_2 provides solid support for $ZnCl_2$. Due to their synergistic effect, nanostructured $ZnCl_2$–TiO_2 can work as an efficient heterogeneous catalyst for the synthesis of propargylamines.

Table 4 Recyclability study of $ZnCl_2$–TiO_2[a]

Run	Yield[b] (%)
1	97
2	94
3	90
4	88
5	84

[a] Reaction conditions: 3-hydroxybenzaldehyde (1 mmol), morpholine (1.2 mmol), phenylacetylene (1.5 mmol), recycled $ZnCl_2$–TiO_2 catalyst, 100 °C, 6.0 h, solvent-free. [b] Isolated yield.

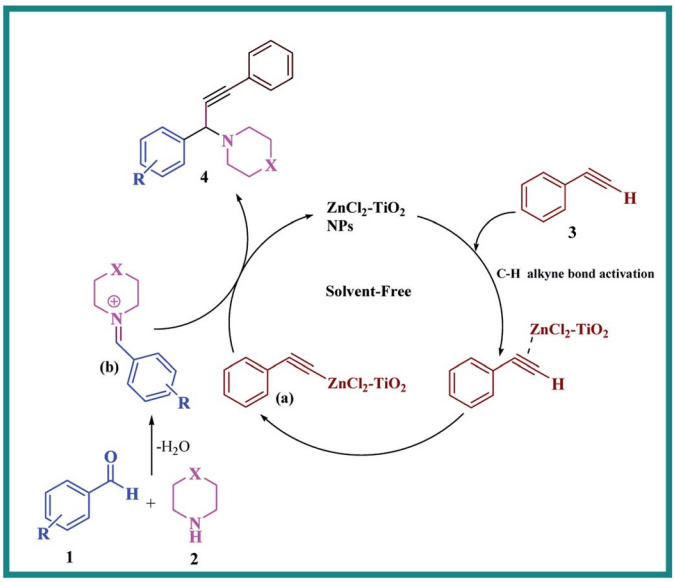

Scheme 3 A tentative mechanism for the synthesis of propargylamine catalysed by $ZnCl_2$–TiO_2 nanoparticles (NPs).

4. Conclusion

We have reported a simple and efficient route for the synthesis of propargylamine using small amount of nanocrystalline $ZnCl_2$–TiO_2 as a heterogeneous catalyst. The role of catalyst is significantly observed for alkyne C–H bond activation. The reported technique is solvent-free and required mild reaction conditions. The synthesized 15% $ZnCl_2$ loaded TiO_2 nanomaterial was found to be an excellent catalyst for the synthesis of diverse propargylamine derivatives. We believe that our present protocol is eco-friendly for green approach and can become an alternative to conventional homogeneous catalysis for the synthesis of propargylamine.

Conflicts of interest

There are no conflicts to declare.

Acknowledgements

D. B. Bankar is obliged to Dr B. B. Kale, Director of C-MET, Pune, India for providing research facility. He is also indebted to the Principal and Head of the Chemistry Department of R. B. Narayanrao Borawake College, Shrirampur, India for support to this research work. Dr K. G. Kanade is thankful to RUSA, India for financial and the Rayat Shikshan Sanstha, Satara, for administrative support. Authors are grateful to the Director of NCL, Pune for providing XPS facility.

References

1 M. Jeganathan, A. Dhakshinamoorthy and K. Pitchumani, *ACS Sustainable Chem. Eng.*, 2014, **2**, 781–787.
2 K. Gong, H. Wang, S. Wang and X. Ren, *Tetrahedron*, 2015, **71**, 4830–4834.
3 A. Teimouri, A. N. Chermahini and M. Narimani, *Bull. Korean Chem. Soc.*, 2012, **33**, 1556–1560.
4 D. S. Ermolat'ev, J. B. Bariwal, H. P. Steenackers, S. C. De Keersmaecker and E. V. Van der Eycken, *Angew. Chem., Int. Ed.*, 2010, **49**, 9465–9468.
5 D. F. Harvey and D. M. Sigano, *J. Org. Chem.*, 1996, **61**, 2268–2272.
6 Y. Yamamoto, H. Hayashi, T. Saigoku and H. Nishiyama, *J. Am. Chem. Soc.*, 2005, **127**, 10804–10805.
7 D. Shibata, E. Okada, J. Molette and M. Medebielle, *Tetrahedron Lett.*, 2008, **49**, 7161–7164.
8 W. J. Yoo and C. J. Li, *Adv. Synth. Catal.*, 2008, **350**, 1503–1506.
9 B. Yan and Y. Liu, *Org. Lett.*, 2007, **9**, 4323–4326.
10 M. L. Kantam, V. Balasubrahmanyam, K. S. Kumar and G. Venkanna, *Tetrahedron Lett.*, 2007, **48**, 7332–7334.
11 C. Binda, F. Hubálek, M. Li, Y. Herzig, J. Sterling, D. E. Edmondson and A. Mattevi, *J. Med. Chem.*, 2004, **47**, 1767–1774.
12 M. Naoi, W. Maruyama, H. Yi, Y. Akao, Y. Yamaoka and M. Shamoto-Nagai, *J. Neural Transm.*, 2007, 121–131.
13 T. K. Saha and R. Das, *ChemistrySelect*, 2018, **3**, 147–169.
14 B. Agrahari, S. Layek, R. Ganguly and D. D. Pathak, *New J. Chem.*, 2018, **42**, 13754–13762.
15 (*a*) V. V. Kouznetsov and L. Y. V. Mendez, *Synthesis*, 2008, **2008**(04), 491–506; (*b*) G. Blay, A. Monleon and J. Pedro, *Curr. Org. Chem.*, 2009, **13**, 1498–1539.
16 E. Ramu, R. Varala, N. Sreelatha and S. R. Adapa, *Tetrahedron Lett.*, 2007, **48**, 7184–7190.
17 Y. Imada, M. Yuasa, I. Nakamura and S.-I. Murahashi, *J. Org. Chem.*, 1994, **59**, 2282–2284.
18 A. Bisai and V. K. Singh, *Org. Lett.*, 2006, **8**, 2405–2408.
19 C. Wei, Z. Li and C.-J. Li, *Org. Lett.*, 2003, **5**, 4473–4475.
20 L. Zani, S. Alesi, P. G. Cozzi and C. Bolm, *J. Org. Chem.*, 2006, **71**, 1558–1562.
21 P. Li, Y. Zhang and L. Wang, *Chem.–Eur. J.*, 2009, **15**, 2045–2049.
22 (*a*) J. Lim, K. Park, A. Byeun and S. Lee, *Tetrahedron Lett.*, 2014, **55**, 4875–4878; (*b*) C. Zhao and D. Seidel, *J. Am. Chem. Soc.*, 2015, **137**, 4650–4653.
23 L. C. Akullian, M. L. Snapper and A. H. Hoveyda, *Angew. Chem., Int. Ed.*, 2003, **42**, 4244–4247.
24 S. Samai, G. C. Nandi and M. Singh, *Tetrahedron Lett.*, 2010, **51**, 5555–5558.
25 Y. Zhang, P. Li, M. Wang and L. Wang, *J. Org. Chem.*, 2009, **74**, 4364–4367.
26 S. Sakaguchi, T. Mizuta, M. Furuwan, T. Kubo and Y. Ishii, *Chem. Commun.*, 2004, 1638–1639.
27 X. Chen, T. Chen, Y. Zhou, C.-T. Au, L.-B. Han and S.-F. Yin, *Org. Biomol. Chem.*, 2014, **12**, 247–250.
28 C.-J. Li and C. Wei, *Chem. Commun.*, 2002, 268–269.
29 J. Yadav, B. S. Reddy, A. H. Gopal and K. Patil, *Tetrahedron Lett.*, 2009, **50**, 3493–3496.
30 W.-W. Chen, H.-P. Bi and C.-J. Li, *Synlett*, 2010, **2010**, 475–479.

31 V. K.-Y. Lo, Y. Liu, M.-K. Wong and C.-M. Che, *Org. Lett.*, 2006, **8**, 1529–1532.
32 M. L. Kantam, B. V. Prakash, C. R. V. Reddy and B. Sreedhar, *Synlett*, 2005, **2005**, 2329–2332.
33 P. Li, L. Wang, Y. Zhang and M. Wang, *Tetrahedron Lett.*, 2008, **49**, 6650–6654.
34 S. Kaur, M. Kumar and V. Bhalla, *Chem. Commun.*, 2015, **51**, 16327–16330.
35 S. Wang, X. He, L. Song and Z. Wang, *Synlett*, 2009, **2009**, 447–450.
36 H. Naeimi and M. Moradian, *Appl. Organomet. Chem.*, 2013, **27**, 300–306.
37 D. Bhuyan, M. Saikia and L. Saikia, *Catal. Commun.*, 2015, **58**, 158–163.
38 K. Satyanarayana, P. A. Ramaiah, Y. Murty, M. R. Chandra and S. Pammi, *Catal. Commun.*, 2012, **25**, 50–53.
39 M. Rahman, A. K. Bagdi, A. Majee and A. Hajra, *Tetrahedron Lett.*, 2011, **52**, 4437–4439.
40 M. L. Kantam, J. Yadav, S. Laha and S. Jha, *Synlett*, 2009, **2009**, 1791–1794.
41 K. Namitharan and K. Pitchumani, *Eur. J. Org. Chem.*, 2010, **2010**, 411–415.
42 K. D. Bhatte, D. N. Sawant, K. M. Deshmukh and B. M. Bhanage, *Catal. Commun.*, 2011, **16**, 114–119.
43 M. J. Albaladejo, F. Alonso, Y. Moglie and M. Yus, *Eur. J. Org. Chem.*, 2012, **2012**, 3093–3104.
44 S. K. Movahed, N. F. Lehi and M. Dabiri, *RSC Adv.*, 2014, **4**, 42155–42158.
45 M. Gholinejad, F. Hamed and C. Najera, *Synlett*, 2016, **27**, 1193–1201.
46 Z. Zarei and B. Akhlaghinia, *RSC Adv.*, 2016, **6**, 106473–106484.
47 S. Layek, B. Agrahari, S. Kumari and D. D. Pathak, *Catal. Lett.*, 2018, **148**, 2675–2682.
48 N. Gharibpour, M. Abdollahi Alibeik and A. Moaddeli, *ChemistrySelect*, 2017, **2**, 3137–3146.
49 A. Moshfegh, *J. Phys. D: Appl. Phys.*, 2009, **42**, 233001.
50 W. Buraso, V. Lachom, P. Siriya and P. Laokul, *Mater. Res. Express*, 2018, **5**, 115003.
51 D. A. Kotadia and S. S. Soni, *Appl. Catal., A*, 2014, **488**, 231–238.
52 Y. M. Mohamed, H. A. El Nazer and E. J. Solum, *Chem. Pap.*, 2019, **73**, 435–445.
53 S. Mishra, A. K. Bagdi, M. Ghosh, S. Sinha and A. Hajra, *RSC Adv.*, 2014, **4**, 6672–6676.
54 U. Sakee and R. Wanchanthuek, *Mater. Res. Express*, 2017, **4**, 115504.
55 M. Ahamed, M. M. Khan, M. J. Akhtar, H. A. Alhadlaq and A. Alshamsan, *Sci. Rep.*, 2016, **6**, 30196.
56 S. Honglong, Z. Guling, Z. Bin, L. Minting and W. Wenzhong, *Microsc. Res. Tech.*, 2013, **76**, 641–647.
57 S. K. M. Saad, A. A. Umar, H. Q. Nguyen, C. F. Dee, M. M. Salleh and M. Oyama, *RSC Adv.*, 2014, **4**, 57054–57063.
58 J. Liqiang, W. Dejun, W. Baiqi, L. Shudan, X. Baifu, F. Honggang and S. Jiazhong, *J. Mol. Catal. A: Chem.*, 2006, **244**, 193–200.
59 A. Abidli, S. Hamoudi and K. Belkacemi, *Dalton Trans.*, 2015, **44**, 9823–9838.
60 L. Dake, D. Baer and J. Zachara, *Surf. Interface Anal.*, 1989, **14**, 71–75.
61 Y. Yu, J. Wang, W. Li, W. Zheng and Y. Cao, *CrystEngComm*, 2015, **17**, 5074–5080.